

Spatial variability of the snowmelt-albedo feedback in Antarctica

Constantijn L. Jakobs¹, Carleen H. Reijmer¹, Michiel R. van den Broeke¹, J. Melchior van Wessem¹, and Willem Jan van de Berg²

¹Utrecht University

²University of Utrecht

November 22, 2022

Abstract

Surface melt is an important process for the stability of ice shelves, and therewith the Antarctic ice sheet. In Antarctica, absorption of solar radiation is mostly the largest energy source for surface melt, which is further enhanced by the snowmelt-albedo feedback (SMAF): refrozen snow has a lower albedo than new snow, which causes it to absorb more solar radiation, further increasing the energy available for surface melt. This feedback has previously been shown to increase surface melt by approximately a factor of 2.5 at Neumayer Station in East Antarctica. In this study, we use a regional climate model to quantify SMAF for the entire Antarctic ice sheet. We find that it is most effective on ice shelves in East Antarctica, and is less important in the Antarctic Peninsula and on the Ross and Filchner-Ronne ice shelves. We identify a relationship between SMAF and average summer air temperatures, and find that SMAF is most important around 265 ± 2 K. On a sub-seasonal scale, we identify several parameters that contribute to SMAF: the length of dry periods, the time between significant snowfall events and snowmelt events, and prevailing temperatures. We then apply the same temperature-dependency of SMAF to the Greenland ice sheet and find that it is potentially active in a narrow band around the ice sheet, and finally discuss how the importance of SMAF could change in a warming climate.

1 **Spatial variability of the snowmelt–albedo feedback in**
2 **Antarctica**

3 **C. L. Jakobs¹, C. H. Reijmer¹, M. R. van den Broeke¹**
4 **W. J. van de Berg¹, J. M. van Wessem¹**

5 ¹Institute for Marine and Atmospheric Research Utrecht, Utrecht University, The Netherlands

6 **Key Points:**

- 7 • We use a regional climate model to quantify the snowmelt–albedo feedback for the
8 Antarctic ice sheet
9 • We find that this feedback is most active on East Antarctic ice shelves
10 • Precipitation frequency, timing and summer air temperature are key parameters
11 for its importance

Corresponding author: Stan Jakobs, c.l.jakobs@uu.nl

Abstract

Surface melt is an important process for the stability of ice shelves, and therewith the Antarctic ice sheet. In Antarctica, absorption of solar radiation is mostly the largest energy source for surface melt, which is further enhanced by the snowmelt–albedo feedback (SMAF): refrozen snow has a lower albedo than new snow, which causes it to absorb more solar radiation, further increasing the energy available for surface melt. This feedback has previously been shown to increase surface melt by approximately a factor of 2.5 at Neumayer Station in East Antarctica. In this study, we use a regional climate model to quantify SMAF for the entire Antarctic ice sheet. We find that it is most effective on ice shelves in East Antarctica, and is less important in the Antarctic Peninsula and on the Ross and Filchner-Ronne ice shelves. We identify a relationship between SMAF and average summer air temperatures, and find that SMAF is most important around 265 ± 2 K. On a sub-seasonal scale, we identify several parameters that contribute to SMAF: the length of dry periods, the time between significant snowfall events and snowmelt events, and prevailing temperatures. We then apply the same temperature-dependency of SMAF to the Greenland ice sheet and find that it is potentially active in a narrow band around the ice sheet, and finally discuss how the importance of SMAF could change in a warming climate.

Plain Language Summary

The Antarctic ice sheet is surrounded by ice shelves: floating extensions that prevent it from flowing into the oceans. The stability of these ice shelves is mainly affected by the melting of snow and ice, leading to a potential disintegration of the entire ice shelf. To properly simulate the climate, models should therefore be able to accurately reproduce snowmelt rates. Snowmelt in Antarctica is mainly driven by the absorption of solar radiation. This is subject to a positive feedback: when snow melts, it becomes darker, causing it to absorb more radiation. This leads to more energy that is available for snowmelt, which further darkens the surface. In this study, we use a climate model to quantify the importance of this feedback for the Antarctic ice sheet. We find that it is most important in regions with an average summer air temperature around 265 K. We furthermore find that during a long, dry period in summer, the feedback is more effective, and that the timing between snowfall and snowmelt partly determines how much the feedback will affect snowmelt. As a final step, we estimate how important this feedback is in Greenland, and how the observed patterns could change in a warming climate.

1 Introduction

The Antarctic ice sheet (AIS) contains approximately 26 million km^3 of ice, equivalent to a global mean sea level change of 58 m (Morlighem et al., 2020). In recent years, accelerated mass loss from the AIS has been observed; Shepherd et al. (2018) report a mass loss rate of 109 ± 56 Gt yr^{-1} over the period 1992–2017. The highest mass loss is observed in West Antarctica, as a result of the thinning and disappearing of ice shelves, the floating extensions of the grounded ice sheet. Ice shelves are present along $\sim 74\%$ of the AIS (Bindschadler et al., 2011), buttressing the grounded ice sheet. They experience basal melt through ocean–ice heat exchange (Pritchard et al., 2012; Massom et al., 2018), as well as surface melt by energy exchange at the ice-shelf surface (Van den Broeke, 2005; Kingslake et al., 2017). The recent collapse of Larsen A and B ice shelves on the east side of the Antarctic Peninsula (AP) was preceded by extensive surface melt, inducing hydrofracturing (Van den Broeke, 2005; Glasser & Scambos, 2008). On the west side of the AP, break-up events on Wilkins ice shelf have been associated with increased basal melt rates, leading to changes in buoyant forces (Braun et al., 2009; Padman et al., 2012). Ice-shelf thinning and break-up have both been associated with the acceleration of its feeding glaciers (Scambos et al., 2004; Rott et al., 2011), causing the high

62 mass loss rates in coastal West Antarctica and the AP (Wouters et al., 2015; Turner et
63 al., 2017). Ice-shelf stability is thus crucial for the future mass balance of the AIS. Be-
64 cause both basal and surface melt are expected to increase in a warming climate also for
65 the more southerly ice shelves (Trusel et al., 2015), a proper representation of ice-shelf
66 melt processes is essential in climate modeling.

67 In this paper we focus on surface melt processes. Weather stations, satellites and
68 climate models have been used to estimate surface melt rates on Antarctic ice shelves
69 (Bromwich et al., 2013; Trusel et al., 2015; Van Kampenhout et al., 2017; Van Wessem
70 et al., 2018; Agosta et al., 2019; Souverijns et al., 2019). In-situ observations show that
71 in the cold climate of Antarctica, insolation is usually the most important energy source
72 for surface melt (Van den Broeke, Reijmer, et al., 2005; Jonsell et al., 2012; King et al.,
73 2015; Jakobs et al., 2020). The absorption of solar radiation is in turn enhanced by the
74 snowmelt–albedo feedback (SMAF) (Jakobs et al., 2019): when snow melts, meltwater
75 percolates into the subsurface snow layers where it can refreeze. As refrozen snow con-
76 sists of larger snow grains than new snow, it reduces the backward scattering of photons
77 (Wiscombe & Warren, 1980), i.e. it has a lower albedo. As a result, the surface absorbs
78 more incoming solar radiation, leading to more surface melt, representing a positive feed-
79 back. Therefore, it is crucial for climate models to use a snow albedo parameterization
80 that includes this melt–albedo feedback (Cullather et al., 2014; Van Dalum et al., 2019;
81 Alexander et al., 2019).

82 In a previous study, we used high-quality meteorological observations from Neu-
83 mayer Station, located on Ekström ice shelf in East Antarctica, to quantify the effect
84 of SMAF on surface melt rates (Jakobs et al., 2019). We used a surface energy balance
85 (SEB) model that includes a grain-size-dependent albedo parameterization, and found
86 that on average, SMAF enhanced surface melt (1992–2016) at Neumayer Station by a
87 factor of 2.5, but with significant interannual variability. The current study aims to ex-
88 tend our previous work to the entire AIS, using the regional climate model RACMO2.
89 This climate model is specifically developed to simulate polar climates and has been ex-
90 tensively evaluated (Van Wessem et al., 2018; Jakobs et al., 2020). Its albedo param-
91 eterization makes it well-suited to study SMAF at the continental scale.

92 In the next section, we introduce the climate model RACMO2 and describe the albedo
93 parameterization used. In Section 3 we present a map of SMAF in Antarctica (Section
94 3.1), discussing its spatial variability as well as the interannual variability at different
95 locations (Section 3.2). We identify regions in Antarctica that are most affected by SMAF
96 (Section 4.1) and present local case studies on a daily timescale to identify conditions
97 where SMAF is largest (Section 4.2). In Section 4.3, we comment on the potential im-
98 portance of SMAF in Greenland, and how SMAF will affect surface melt in the future
99 on both ice sheets, followed by conclusions in Section 5.

100 **2 Methods**

101 **2.1 Model descriptions**

102 The regional climate model RACMO2 is developed by the Royal Netherlands Me-
103 teorological Institute (KNMI). It is a hydrostatic model that combines the dynamical
104 core of the High Resolution Limited Area Model (HIRLAM, Undén et al. (2002)) with
105 the physics parameterizations of the Integrated Forecast System (IFS, version CY33r1)
106 of the European Centre for Medium-Range Weather Forecast (ECMWF) (ECMWF, 2008).

107 For this study, we use the latest polar version (RACMO2.3p2, from now on referred
108 to as RACMO2), which has been specifically developed for use over glaciated regions (Reijmer
109 et al., 2005; Van Wessem et al., 2018). The atmosphere is represented by 40 vertical lev-
110 els and the model is forced by the ERA-Interim reanalysis product at its lateral bound-
111 aries as well as in the upper atmosphere (Van de Berg & Medley, 2016). The atmospheric

112 component is coupled to a multilayer snow model (Ettema et al., 2010), which allows for
 113 meltwater percolation, refreezing and runoff. Furthermore, RACMO2 uses an albedo pa-
 114 rameterization that depends on grain size (Gardner & Sharp, 2010; Kuipers Munneke
 115 et al., 2011) and a drifting-snow scheme that simulates horizontal transport of snow by
 116 near-surface winds (Lenaerts et al., 2012).

117 Van Wessem et al. (2018) compared the output of RACMO2 with in-situ measure-
 118 ments of surface temperature, radiation fluxes, turbulent fluxes and wind speed. They
 119 found that RACMO2 yields reliable estimates of surface temperatures and net short-wave
 120 radiation ($R^2 > 0.9$), and performs adequately in modeling turbulent fluxes, net long-
 121 wave radiation and wind speed ($R^2 > 0.5$). They furthermore found a good correla-
 122 tion ($R^2 = 0.81$) of surface melt rates with the results from the QuikSCAT satellite.
 123 Jakobs et al. (2020) showed that RACMO2 reproduces surface melt rates with reason-
 124 able accuracy: compared to in-situ melt estimates from (automatic) weather stations in
 125 the AP and Dronning Maud Land, RACMO2 slightly underestimates surface melt rates
 126 (bias=-7.3 mm w.e. yr⁻¹) but overall, the agreement is good ($R^2 > 0.8$).

127 RACMO2 solves the surface energy balance (SEB) equation, which describes the
 128 energy exchange between the surface, the sub-surface and the atmosphere and determines
 129 the amount of energy available for surface melt:

$$M = R_{\text{net}} + Q_S + Q_L + Q_G, \quad (1)$$

130 where R_{net} is net radiation, the sum of net short-wave and net long-wave radiation, Q_S
 131 and Q_L are the turbulent fluxes of sensible and latent heat, respectively, and Q_G is the
 132 surface value of the subsurface heat flux. M is the energy available for surface melt, which
 133 is equal to 0 when the surface temperature is below the melting point of ice (273.15 K).
 134 In an iterative procedure, the surface temperature is determined so that the SEB is closed.
 135 If this temperature would exceed 273.15 K, it is forced to this value and excess energy
 136 is available for surface melt. The turbulent fluxes Q_S and Q_L are determined using Monin-
 137 Obukhov similarity theory, which relates the fluxes to the near-surface gradients of wind
 138 speed, potential temperature and humidity (see e.g. Van den Broeke, Van As, et al. (2005)).
 139 The subsurface heat flux $Q_G = k \frac{\partial T}{\partial z}$, where k is the effective thermal conductivity of
 140 the snow/ice and $\frac{\partial T}{\partial z}$ the temperature gradient in the near-surface snowpack. The snow
 141 model solves the heat-conductivity equation to obtain the subsurface temperature pro-
 142 file and therewith Q_G (Ettema et al., 2010):

$$\rho c_p \frac{\partial T}{\partial t} = - \frac{\partial}{\partial z} \left(k \frac{\partial T}{\partial z} \right) + q_{\text{refr}}, \quad (2)$$

143 where q_{refr} is the energy released by the refreezing of meltwater per unit time per area.
 144 Penetration of short-wave radiation is not considered in this version of RACMO2.

145 This version of RACMO2 uses the albedo parameterization of Gardner and Sharp
 146 (2010), in which the albedo is described as a base value α_S with modifications due the
 147 solar zenith angle θ ($d\alpha_u$), the cloud optical thickness τ ($d\alpha_\tau$) and the concentration of
 148 black carbon in the snow ($d\alpha_c$). The impact of snow impurities is assumed negligible for
 149 Antarctica and thus $d\alpha_c=0$ (Warren & Clarke, 1990; Grenfell et al., 1994; Bisiaux et al.,
 150 2012; Marquetto et al., 2020)).

151 The base albedo α_S is given by (Gardner & Sharp, 2010):

$$\alpha_S = 1.48 - 1.27048 r_e^{0.07}, \quad (3)$$

152 where r_e is the snow grain size, in turn parameterized as

$$r_e(t) = [r_e(t-1) + dr_{e,\text{dry}} + dr_{e,\text{wet}}] f_o + r_{e,0} f_n + r_{e,r} f_r, \quad (4)$$

153 where $dr_{e,\text{dry}}$ and $dr_{e,\text{wet}}$ describe grain growth due to dry and wet snow metamorphism,
 154 respectively. $r_{e,0}$ and $r_{e,r}$ denote the grain sizes of new and refrozen snow, set to con-
 155 stant values of $r_{e,0} = 54$ mm (Kuipers Munneke et al., 2011) and $r_{e,r} = 1000$ mm (Van Wessem

156 et al., 2018). f_o , f_n and f_r are the fractions of old, new and refrozen snow. The effect
 157 of the second layer is considered by changing the base albedo α_S to:

$$\alpha'_S = (\alpha_S^{\text{btm}} - \alpha_S^{\text{top}}) + A(\alpha_S^{\text{top}} - \alpha_S^{\text{btm}}), \quad (5)$$

158 where top and btm indicate the top and bottom layers respectively, and A is a factor de-
 159 pendent on α_S^{top} and the top-layer thickness z . Equations for $d\alpha_u$, $d\alpha_\tau$, $dr_{e,\text{dry}}$, $dr_{e,\text{wet}}$
 160 and A can be found in Gardner and Sharp (2010). This approach is different from Kuipers Munneke
 161 et al. (2011) and Jakobs et al. (2019), who used more than two layers to calculate the
 162 surface albedo.

163 2.2 Quantifying SMAF

164 To quantify the effect of SMAF, we performed two simulations with RACMO2 on
 165 a 27 km horizontal resolution for the period 1979–2018: a baseline run R_0 in which the
 166 full albedo parameterization is used as described above, and a sensitivity run R_1 , in which
 167 the contribution of refrozen snow to snow grain size, and hence surface albedo, is dis-
 168 abled by setting $f_r = 0$ in Eq. (4). The same approach was used by Jakobs et al. (2019)
 169 to quantify SMAF at Neumayer Station in East Antarctica. The term ‘period-average’
 170 is used throughout this article, referring to the period 1979–2018.

171 There are several ways to quantify SMAF. The most robust definition is SMAF_t ,
 172 the ratio of the total (‘t’) cumulative amounts of surface melt in R_0 and R_1 over the en-
 173 tire period available (in this study 1979–2018). We use this measure to interpret the spa-
 174 tial variability of SMAF and e.g. its correlation with period-average temperature. SMAF
 175 can also be determined on a seasonal (‘s’) basis, i.e. the ratio of seasonal (in this study
 176 Jul–Jun) melt in R_0 and R_1 , and is denoted by SMAF_s . Time series of SMAF_s are used
 177 to study the interannual variability of SMAF and the connection to the SEB.

178 3 Results

179 3.1 Spatial distribution of SMAF

180 Since SMAF is defined as the ratio of surface melt in two different runs, we first
 181 present the relation between seasonal surface melt rates and SMAF_s in Fig. 1a, for sea-
 182 sons with at least 10 mm w.e. of surface melt, for each model grid cell. The figure shows
 183 that the highest SMAF_s values occur in low-melt regions, while in high-melt regions SMAF_t
 184 is close to 1. It furthermore shows that melt is not the only driver of SMAF_s . In this sec-
 185 tion we study the spatial distribution of SMAF and surface melt; in Sect. 4 we then dis-
 186 cuss possible other drivers of SMAF.

187 To identify the regions where SMAF is most important, we first need to know the
 188 spatial distribution of surface melt in Antarctica. This is presented in Fig. 2a, with the
 189 highest values occurring on both sides of the AP, locally exceeding $300 \text{ mm w.e. yr}^{-1}$. Ex-
 190 treme values ($>500 \text{ mm w.e. yr}^{-1}$) occur on small islands north of the AP. The highest
 191 surface melt rates in East Antarctica are found on Shackleton ice shelf (indicated in Fig. 2c
 192 with an ‘S’), due to its northerly location. The lowest values are found on the Ross and
 193 Filchner-Ronne ice shelves. The absolute increase in seasonal average melt because of
 194 SMAF ($R_0 - R_1$) is shown in Fig. 2b. A pattern similar to Fig. 2a emerges, with the
 195 highest values in the AP and on Shackleton ice shelf, but also in coastal Dronning Maud
 196 Land and the Amundsen Sea sector.

197 Figure 2c shows the resulting SMAF_t , ranging from 1 to ~ 2.8 , for locations with
 198 at least 5 mm w.e. of period-average seasonal surface melt. The highest values are found
 199 in coastal Dronning Maud Land and the Amundsen Sea sector; these locations have rela-
 200 tively low seasonal surface melt rates, combined with an increase because of SMAF that
 201 is relatively large. Lower values are found in low-melt regions such as on the Ross and

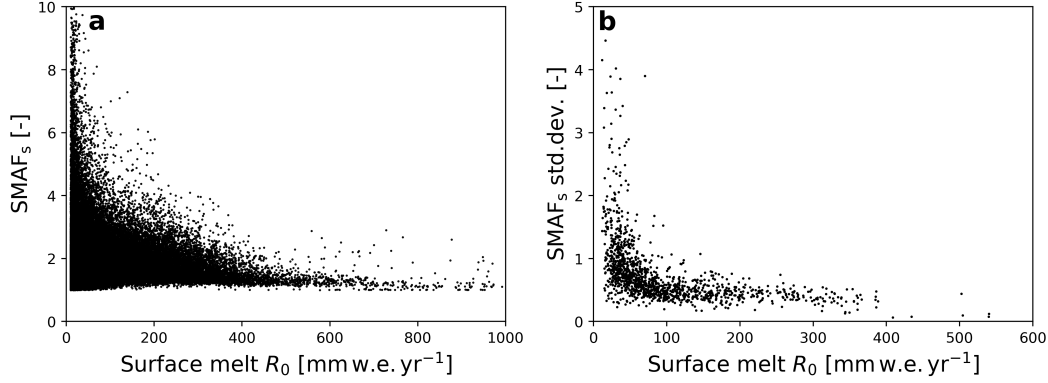


Figure 1. **a** Relationship between surface melt rate and SMAF_s . Each dot represents one season with at least 10 mm w.e. for all grid points within the model domain. **b** Period-average seasonal surface melt versus SMAF_s standard deviation for all grid points with period-average seasonal surface melt ≥ 5 mm w.e.

202 Filchner-Ronne ice shelves, and high-melt regions such as the northern AP. These pat-
 203 terns are discussed in more detail in Sect. 4.1, but first we consider the temporal vari-
 204 ability of SMAF_s .

205 3.2 Temporal variability of SMAF

206 For six locations, indicated by blue dots in Fig. 2c, time series of seasonal snow melt
 207 for both runs (R_0 and R_1) are presented in Fig. 3. The ratio between these two yields
 208 the seasonal SMAF_s value; indicated in top-right are SMAF_t and the average and stan-
 209 dard deviation of SMAF_s . The average of SMAF_s is greater than SMAF_t ; this is a re-
 210 sult of the lower limit of SMAF_s , which is by definition 1. Especially in low-melt regions,
 211 summers with high SMAF_s have a larger effect on its average than on SMAF_t .

212 These locations were selected to illustrate the different SMAF regimes. On Larsen
 213 C ice shelf (Fig. 3f), SMAF leads to an increase in surface melt by a relatively constant
 214 factor every year, characterized by a low standard deviation of SMAF_s . This is differ-
 215 ent from e.g. Amery ice shelf (Fig. 3c), where SMAF_s varies strongly from year to year
 216 (high standard deviation of SMAF_s). For the other locations, the standard deviation ranges
 217 between these extremes. Note that Larsen C and King Baudouin ice shelves have sig-
 218 nificant melt events outside of the summer months, because of regular Föhn events (Lenaerts
 219 et al., 2017; Wiesenekker et al., 2018). These are however not sensitive to SMAF, as they
 220 are not driven by short-wave radiation but rather by turbulent heat fluxes.

221 Figure 1b shows a decrease of SMAF_s interannual variability with increasing melt.
 222 In low-melt regions (< 100 mm w.e. yr^{-1}), melt is highly intermittent and the albedo
 223 remains generally high. If melt occurs, the albedo decreases significantly and surface melt
 224 increases relatively strongly, yielding large SMAF_s values. In contrast, high-melt regions
 225 have a lower surface albedo to start with due to the higher prevailing temperatures; the
 226 albedo-lowering effect of melt is therefore less influential and melt is only slightly enhanced,
 227 leading to low SMAF_s values and variability.

228 Figures 1 and 2 present the relationship between surface melt and SMAF. How-
 229 ever, these figures also suggest there are more drivers determining SMAF. These are the
 230 subject of Sect. 4.1, where we identify climatic regions where SMAF is most active. Sec-

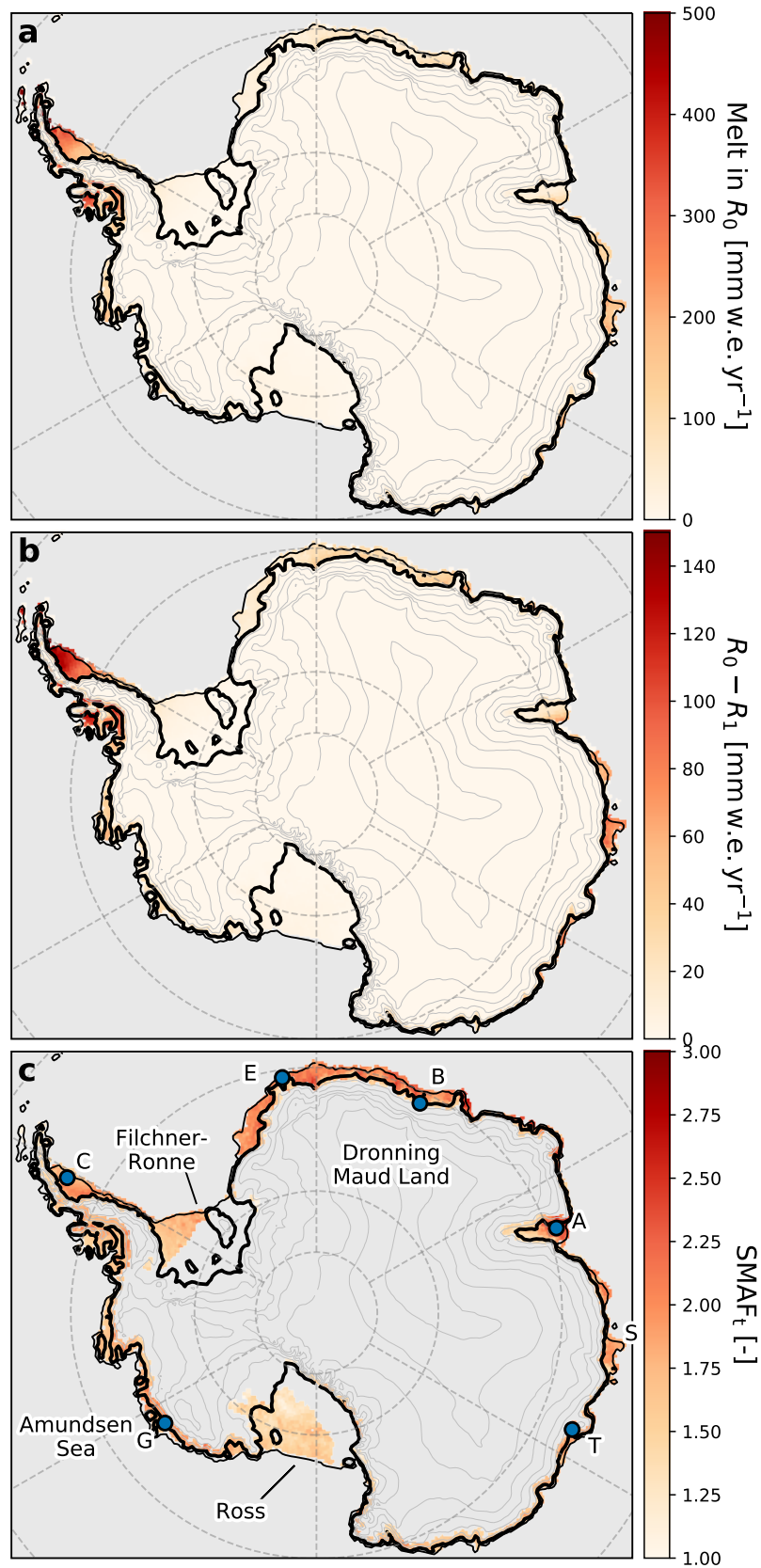


Figure 2. (a) Period-average seasonal surface melt rates modeled by RACMO2, with the full albedo parameterization (run R_0). (b) Difference in average seasonal surface melt rates between runs R_0 and R_1 . (c) SMAF_t for all grid points with period-average seasonal surface melt $\geq 5 \text{ mm w.e.}$ Blue dots indicate sites for which Fig. 3 presents time series of surface melt: Ekström (E), King Baudouin (B), Amery (A), Totten (T), Getz (G) and Larsen C (C) ice shelves. Shackleton ice shelf is indicated with an S.

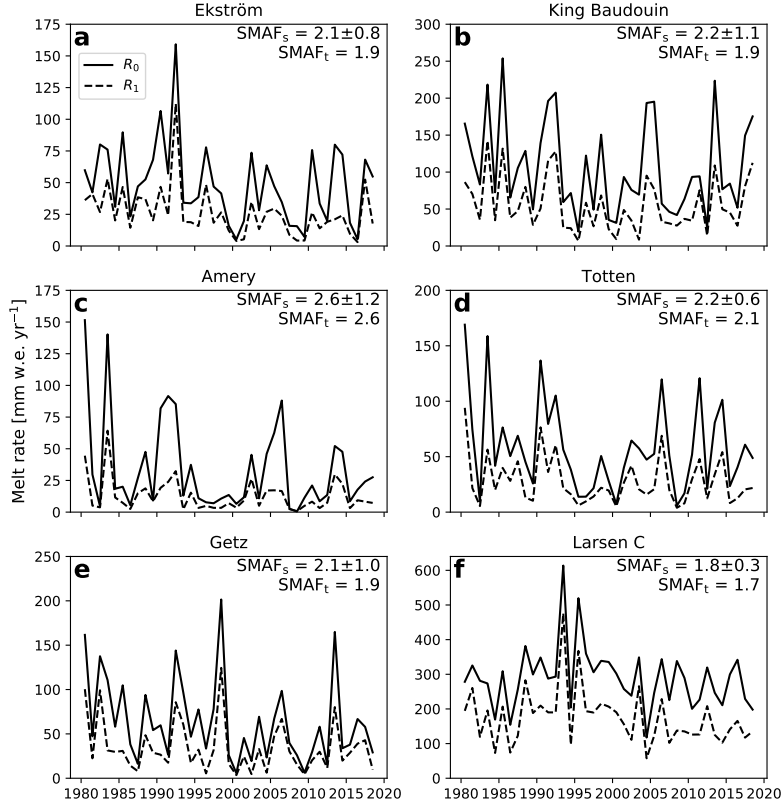


Figure 3. Time series of seasonal surface melt rates at various ice shelves around the Antarctic ice sheet (see Fig. 2c). Melt in R_0 is indicated with a solid line, in R_1 with a dashed line; the ratio between the two gives the seasonal SMAF_s value. Numbers in the top right corner are SMAF_t , the average of SMAF_s and its standard deviation.

231 tion 4.2 focusses on how SMAF is related to the SEB on a daily timescale, for different
 232 regimes.

233 4 Discussion

234 4.1 Climatic drivers of SMAF

235 To understand the spatial patterns in Fig. 2c, we investigated the relationship be-
 236 tween SMAF_t and several quantities: summer (Nov–Feb) air temperature, summer pre-
 237 cipitation and seasonal surface melt rate. The most discernible pattern is observed in
 238 the correlation with temperature, which is therefore used below to describe large-scale
 239 climate drivers of SMAF_t . Precipitation and surface melt are used to discuss SMAF on
 240 a sub-seasonal scale in Sect. 4.2.

241 Figure 4 presents the relation between SMAF_t and mean summer air temperature.
 242 It shows that the highest SMAF_t values are found in regions with an average summer
 243 air temperature of ~ 265 K (defined as T_c), where SMAF_t reaches an average value of 1.9.
 244 This pattern is not very sensitive to the chosen period; it is similar if the time period
 245 is limited to an arbitrary 10-year or 20-year period throughout the total period (not shown).
 246 Its shape suggests a ‘peak bandwidth’ rather than a single peak value. Therefore, in the
 247 following we consider a 2 K bandwidth around T_c , i.e. $T_c = 265 \pm 2$ K.

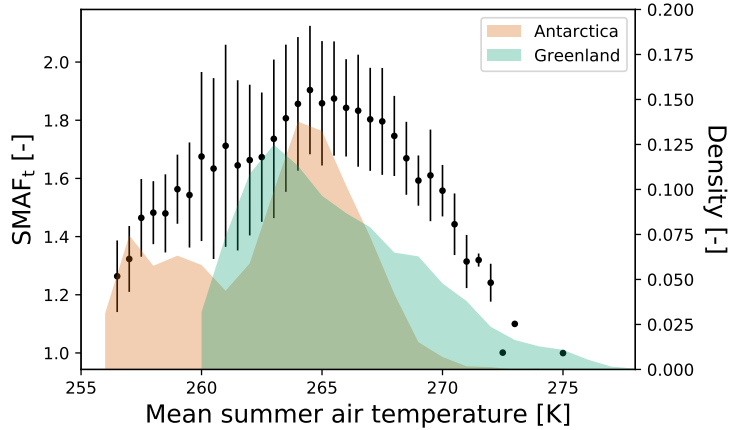


Figure 4. SMAF_t as a function of binned (0.5 K) Nov–Feb average air temperature for all grid points with period-average seasonal surface melt of at least 5 mm w.e (black dots, lines indicate the standard deviation; the three rightmost dots have no lines because there is only 1 data point within the temperature bin). **Right axis** The shading indicates the normalized distribution of average summer air temperature for all grid points with period-average seasonal surface melt of at least 5 mm w.e. in Antarctica (orange, Nov–Feb) and in Greenland (green, accumulation zone only, May–Aug, Noël et al. (2018)).

248 In regions with temperatures above or below T_c , SMAF_t gradually decreases to 1.
 249 In the colder regions ($T < 263$ K), surface melt rates are generally low (mostly < 30 mm w.e. yr $^{-1}$)
 250 and SMAF only moderately enhances surface melt (~ 40 – 50%). In warmer regions ($T >$
 251 267 K), such as the AP, SMAF is also less important for surface melt; due to the rela-
 252 tively mild conditions, the contribution of turbulent heat fluxes is more important to melt
 253 energy than absorption of short-wave radiation. This causes melt events that are less af-
 254 fected by the surface albedo, limiting the influence of SMAF. This is discussed in more
 255 detail in Sect. 4.2.

256 Figure 5 shows the spatial distribution of the deviation of average summer air tem-
 257 perature from T_c in Antarctica (Fig. 5a) and Greenland (Fig. 5b, Noël et al. (2018), dis-
 258 cussed in Sect. 4.3). The Ross, Filchner-Ronne and Amery ice shelves extend far to the
 259 south and are the coldest areas which experience surface melt in Antarctica, with av-
 260 erage summer air temperatures of 260 K and lower. These ice shelves represent the left
 261 tail of the temperature– SMAF_t relation (Fig. 4), where SMAF has a limited effect on
 262 surface melt rates. The AP is the warmest region of Antarctica, with average summer
 263 air temperatures of 270 K and higher. It is located in the right tail of the temperature–
 264 SMAF_t relation, where surface melt is semi-continuous, mainly driven by high air tem-
 265 peratures, and SMAF is also of limited importance for surface melt rates.

266 The remaining, smaller ice shelves in East and West Antarctica experience aver-
 267 age summer air temperatures around T_c , displayed in white in Fig. 5a, with the 2 K band-
 268 width indicated with red contours. This indicates that SMAF is currently significantly
 269 (\sim doubling) enhancing surface melt on ice shelves all around the AIS. In this high-SMAF
 270 regime, surface melt is an intermittent process; the meteorological circumstances that
 271 favor SMAF are identified in the next section.

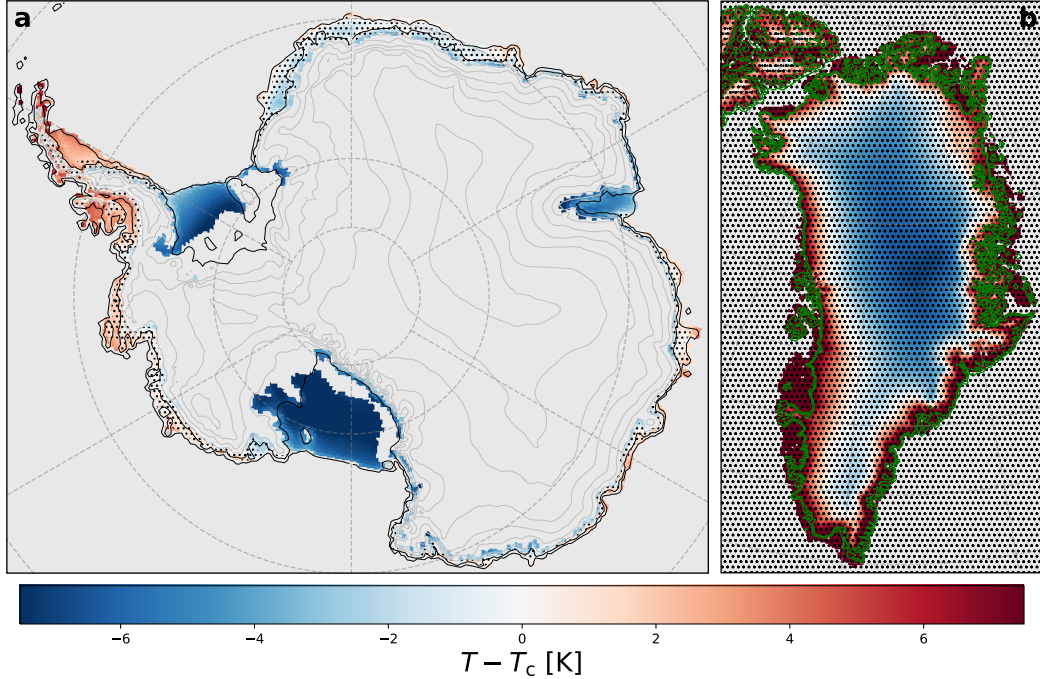


Figure 5. Temperature deviation from $T_c \equiv 265$ K, the temperature at which SMAF plateaus (see Fig. 4), for Antarctica (a) and Greenland (b). Blue areas indicate regions where SMAF will become increasingly important when air temperatures rise. White areas indicate regions where SMAF is now enhancing surface melt the most. Red areas indicate regions where air temperatures / melt are too high for an optimal SMAF. Black dots indicate the 2K bandwidth around T_c , the green contour in (b) indicates the ice sheet margin (Noël et al., 2018).

272

4.2 SMAF and its connection to the SEB

273

274

275

276

277

278

To investigate SMAF and its drivers more closely, we compare summers with different SMAF values at four locations: King Baudouin ice shelf, Ross ice shelf, Larsen C ice shelf and Amery ice shelf (see Fig. 2c for locations). These locations were selected because they represent different SMAF regimes: moderate temperature, strong SMAF (King Baudouin, Fig. 6), high temperature, weak SMAF (Larsen C, Fig. 7), low temperature, weak SMAF (Ross, Fig. 8), and low temperature, strong SMAF (Amery, Fig. 9).

279

280

281

282

283

284

285

286

287

288

289

290

291

292

Figure 6 shows melt-season time series for a location on King Baudouin ice shelf, located in coastal Dronning Maud Land, (indicated by ‘B’ in Fig. 2c) in a moderate-temperature, strong-SMAF region (Fig. 5a). Figure 3b has shown that in this location, $SMAF_s$ experiences a large interannual variability. Figure 6 shows daily cumulative surface melt (a,e), precipitation (b,f), the surface energy balance components (SEB, c,g) and temperature and albedo (d,h) for experiments R_0 and R_1 (see Sect. 2.2). In the melt season 2002–03, around 15 Dec, a melt episode occurs immediately after a strong precipitation event (Fig. 6a and b). Because of refreezing, the albedo drops from 0.9 to ~ 0.75 (Fig. 6d). As no more significant snowfall events follow, the albedo remains low for the remainder of the season, resulting in significantly elevated SW_{net} values (Fig. 6c) and a prolonged period of surface melt in R_0 . The surface albedo is not reset to that of new snow until the end of the melt season. As grain growth by refreezing is inactive in R_1 , the decrease in albedo after the melt event is smaller; it stabilizes at ~ 0.82 . As the surface now reflects more solar radiation, SW_{net} is significantly lower and melt ceases af-

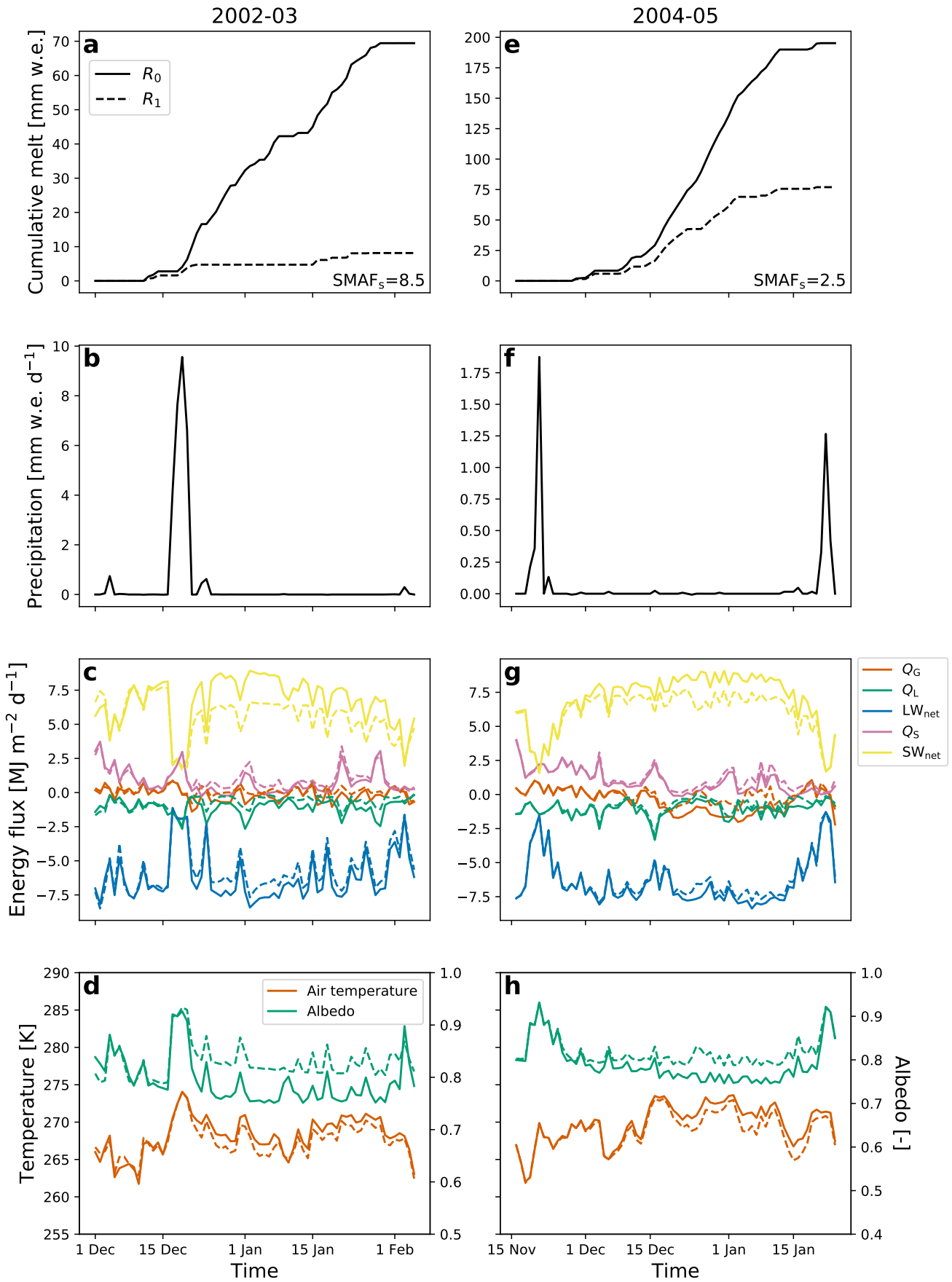


Figure 6. Time series of daily totals of **a,e** surface melt, **b,f** precipitation, **c,g** fluxes of surface energy balance components, and **d,h** average temperature and surface albedo, during the summer of 2002–03 (**a–d**) and 2004–05 (**e–h**) at King Baudouin ice shelf, Dronning Maud Land, East Antarctica (see Fig. 2c, indicated by B). In all panels solid lines indicate R_0 and dashed lines indicate R_1 .

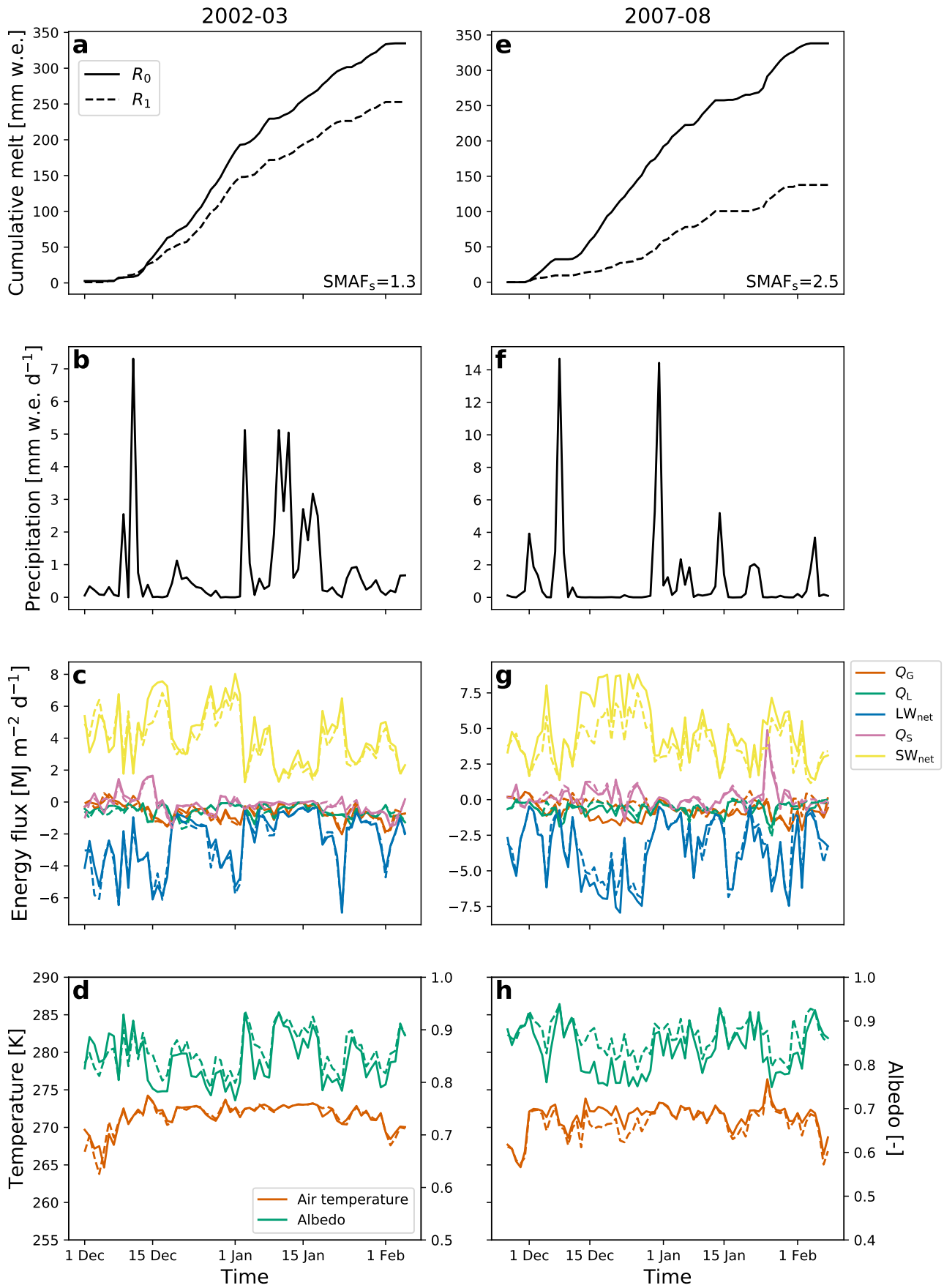


Figure 7. Same as Fig. 6 for Larsen C ice shelf, Antarctic Peninsula (see Fig. 2c, indicated by C).

293 ter the first melt event following the precipitation event. In R_0 melt totaled ~ 70 mm w.e.
 294 during this season, while in R_1 it totaled only 8 mm w.e., yielding a high SMAF_s value
 295 of 8.5 (Fig. 6a).

296 At the same location but two seasons later (2004–05), a similar dry period occurred
 297 (Fig. 6e–h). Contrary to 2002–03, melt did not start immediately after the last signif-
 298 icant snowfall event. Rather, the albedo decreases steadily because of dry snow meta-
 299 morphism in both R_0 and R_1 . Before the first melt of the season, the albedo had decreased
 300 to ~ 0.82 in both runs. Similar to 2002–03, the albedo decreases more in R_0 than in R_1
 301 during the melt event. However the effect of SMAF is now less pronounced than in 2002–
 302 03 because the albedo was already lowered, making the additional contribution of refrozen
 303 snow less important. The difference in SW_{net} is therefore also smaller, as well as the dif-
 304 ference in surface melt rates throughout the season. The total 2004–05 surface melt amounts
 305 are ~ 200 mm w.e. in R_0 and ~ 80 mm w.e. in R_1 , giving a SMAF_s of 2.5 (Fig. 6e).

306 Figure 7 shows results for a location on Larsen C ice shelf in the AP (indicated by
 307 ‘C’ in Fig. 2c), a region that experiences relatively high surface melt rates and higher
 308 temperatures than King Baudouin ice shelf, due to its more northerly location. Melt is
 309 enhanced by SMAF most efficiently between 15 Dec 2007 and 1 Jan 2008, during a pro-
 310 longed dry period (Fig. 7e and f). The subsequent difference in albedo (Fig. 7h) resulted
 311 in significantly more absorption of solar radiation during this period (Fig. 7g) while tem-
 312 peratures were high enough to sustain surface melt. The absence of such a dry period
 313 in 2002–03 prevented SMAF from affecting surface melt as efficiently. Furthermore, the
 314 air temperature is close to the melting point throughout the season, which allowed sus-
 315 tained surface melt in both R_0 and R_1 runs. In the end, SMAF enhanced surface melt
 316 by only $\sim 30\%$ compared to $\sim 140\%$ in 2007–08, which again underlines the importance
 317 of dry periods for the effectiveness of SMAF. The effect is considerably smaller than on
 318 King Baudouin ice shelf (Fig. 6) because of the higher temperature on Larsen C, which
 319 allows for surface melt to proceed even in the absence of SMAF (R_1). This also explains
 320 the smaller interannual variability that is observed in Fig. 3f.

321 Figure 8 shows results for a location on Ross ice shelf, the largest ice shelf in Antarc-
 322 tica (see Fig. 2c). Due to its southerly location, temperatures are significantly lower than
 323 on King Baudouin ice shelf and, therefore, melt is more intermittent and less extensive.
 324 Although in 2007–08 (Fig. 8e–h) the air temperature occasionally reaches the melting
 325 point, sustained melt does not occur. Melt is limited to short melt events during which
 326 SMAF is unable to enhance surface melt over a longer period. However, because melt
 327 energies are so low, small absolute melt differences still induce a significant SMAF_s value
 328 for this season. In another year (2002–03), there was one significant melt event without
 329 any melt enhancement because of SMAF (Fig. 8a). Figure 8c shows that during the melt
 330 event, both SW_{net} and LW_{net} are approaching zero, indicating heavily overcast condi-
 331 tions. Melt energy is for an important part provided by Q_S , which is insensitive to sur-
 332 face albedo. As a result, SMAF did not enhance surface melt during this event.

333 Figure 9 shows daily melt, precipitation, SEB, temperature and albedo for a loca-
 334 tion on Amery ice shelf, East Antarctica (indicated by ‘A’ in Fig. 2c), which experiences
 335 relatively low average temperatures for its latitude. The first season (panels a–d) rep-
 336 represents the high-SMAF summer 2004–05 without a prolonged dry period; even the pre-
 337 cipitation event on 30 Dec was not able to sufficiently reset the surface albedo. During
 338 this event, melt continued because of the persistent high temperature and with it high
 339 Q_S . As a result the new snow was quickly removed from the surface. The difference in
 340 SW_{net} in the following days is sufficient to cause high SMAF_s . In the summer of 2005–
 341 06 (panels e–h) an even higher SMAF_s occurs, resulting from a long dry episode. A re-
 342 markably large difference in air temperature is observed (Fig. 9h) during the persistent
 343 melt episode in R_0 which is absent in R_1 . This is caused by persistently higher surface
 344 temperatures, following larger SW_{net} and refreezing.

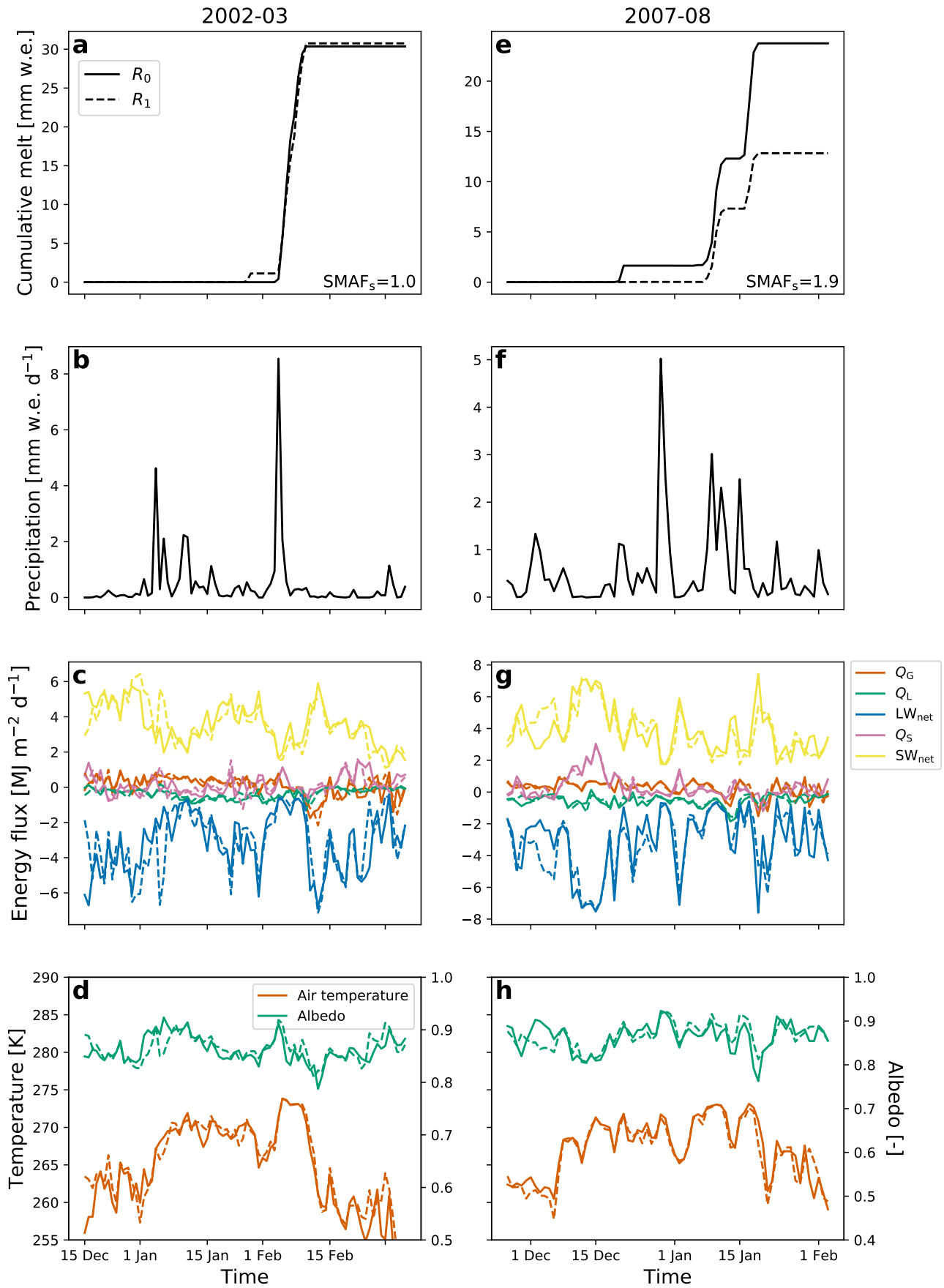


Figure 8. Same as Fig. 6 for Ross ice shelf (see Fig. 2c).

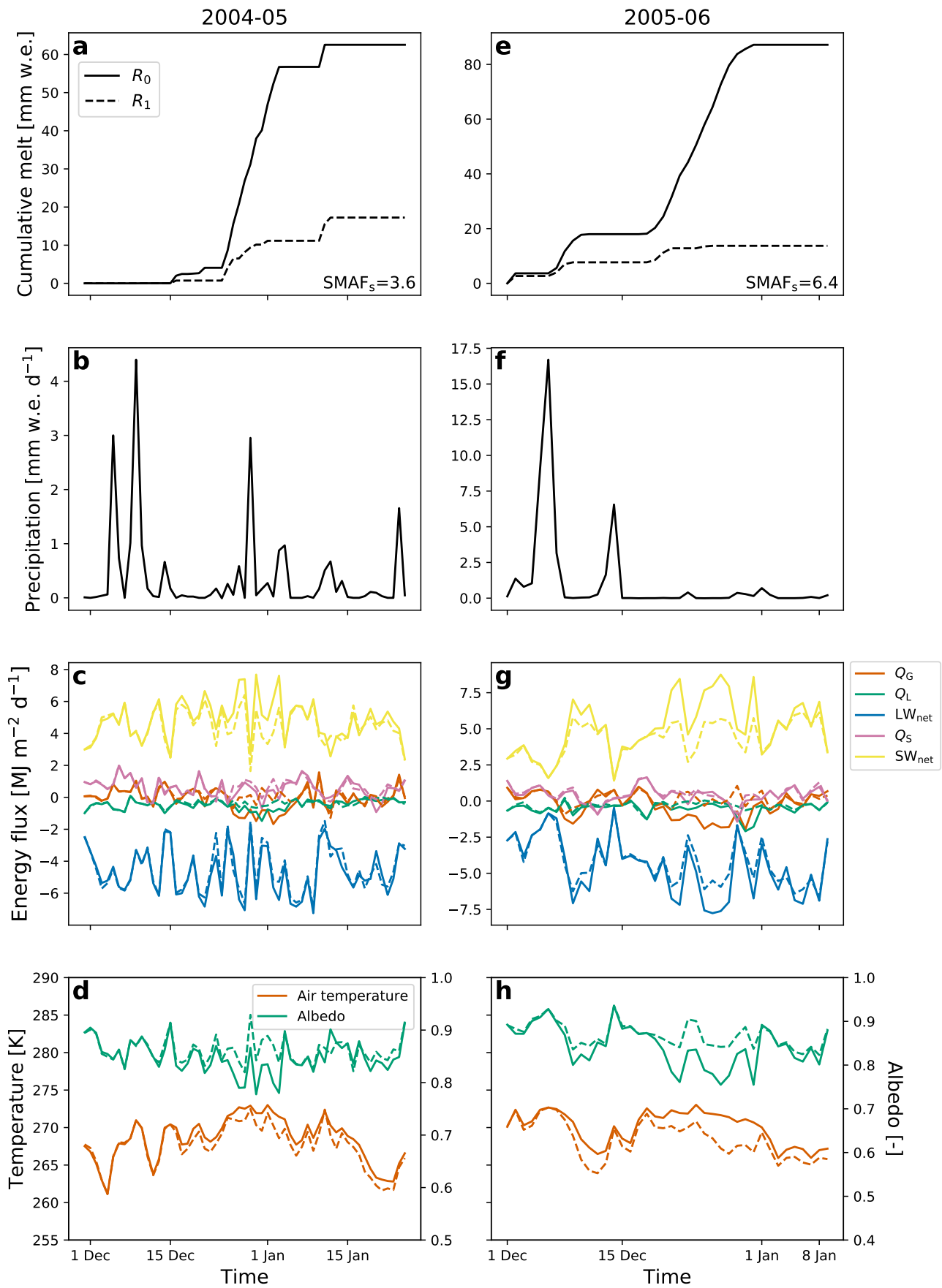


Figure 9. Same as Fig. 6 for Amery ice shelf, Dronning Maud Land (see Fig. 2c, indicated by A).

345 These examples show the different meteorological circumstances that can lead to
 346 different SMAF values. The moderate-temperature regions have the highest SMAF_t val-
 347 ues, because SMAF causes the albedo to be lowered sufficiently such that enhanced ab-
 348 sorption of solar radiation causes continuous melt, which is absent in R_1 . In warm re-
 349 gions, even in cases when the albedo is higher, melt continues in R_1 (see Fig. 7d). Fi-
 350 nally, in cold regions, sustained melt does not occur because of the low temperatures.
 351 Melt is limited to single-day melt events instead, rendering SMAF unable to enhance sur-
 352 face melt for a prolonged period, resulting in small SMAF_s and SMAF_t values.

353 These examples illustrate that especially prolonged dry periods in temperate sum-
 354 mer climates enable SMAF to greatly enhance summer melt amounts, due to the lack
 355 of snowfall resetting the surface albedo. Quantifying the correlation between dry peri-
 356 ods and SMAF_s remains difficult. The exact timing of precipitation and early melt events
 357 is equally important: when dry snow metamorphism has already lowered the surface albedo
 358 before surface melt starts, SMAF is strongly reduced.

359 We conclude that, in order to properly simulate the Antarctic melt climate, a cli-
 360 mate model must accurately represent surface albedo, precipitation timing and inten-
 361 sity, and air and snow temperature.

362 4.3 Outlook: Greenland and the future

363 The shaded areas in Fig. 4 indicate the normalized distributions of temperature
 364 for all grid points with period-average seasonal surface melt of at least 1 mm w.e. in Antarc-
 365 tica (orange) and in Greenland (green, accumulation zone only, Noël et al. (2018)). The
 366 Ross, Filchner-Ronne and Amery ice shelves correspond to the left peak of this distri-
 367 bution, where the impact of SMAF on surface melt rates is limited (Sect. 4.1). The right
 368 peak of this temperature distribution represents the remaining ice shelves along East and
 369 West Antarctica. The higher temperatures are a result of their more northerly location
 370 than the Ross, Filchner-Ronne and Amery ice shelves. This shows that in the current
 371 climate, the majority of melt points fall in a regime with moderate SMAF, with only few
 372 locations significantly above T_c .

373 In a warmer climate, the distributions in Fig. 4 will shift towards the right. The
 374 East Antarctic ice shelves, located in the right peak of the orange distribution, will slowly
 375 become less affected by SMAF. On the other hand, the Ross, Filchner-Ronne and Amery
 376 ice shelves, which are in the left peak of this distribution, will gradually be exposed to
 377 higher SMAF values. As SMAF will become more important on these ice shelves, sur-
 378 face melt will increase relatively more strongly in these regions than for example on coastal
 379 Dronning Maud Land ice shelves. This might negatively affect the stability of the ice shelves
 380 through processes such as increased firn saturation, increased ice temperatures and hy-
 381 drofracturing, and therewith affects the future of the AIS (Trusel et al., 2015).

382 The temperature distribution of melt points in Greenland is shown in green shad-
 383 ing in Fig. 4 (accumulation zone only, Noël et al. (2018)). The absence of large, flat ice
 384 shelves results in large differences with the distribution of Antarctica. The bulk of the
 385 Greenland distribution is centered around 260 K, which represents the high and flat in-
 386 terior accumulation zone. Figure 10 shows the melt–temperature relation for Antarctica
 387 and Greenland (accumulation zone only), relating the period-average summer melt and
 388 summer temperature (Nov–Feb for Antarctica, May–Aug for Greenland). The Green-
 389 land curve seems to be an extension of the Antarctica curve, suggesting that when tem-
 390 peratures increase in the southern hemisphere, the Antarctic melt climate will increas-
 391 ingly resemble the contemporary Greenland melt climate. Note also that the temperature–
 392 SMAF relationship (Fig. 4) is not very sensitive to the time period for which it is cal-
 393 culated (not shown). This suggests that this relationship might also be applicable to Green-
 394 land. In order to assess how SMAF might affect surface melt in Greenland, we there-

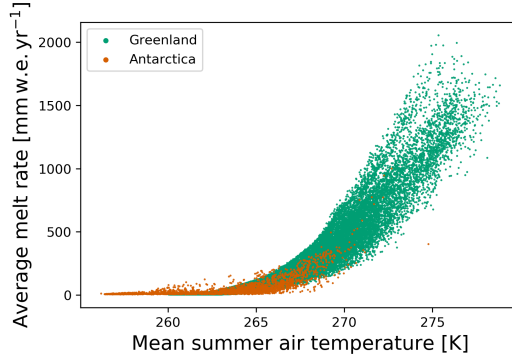


Figure 10. Period-average summer air temperature versus average seasonal surface melt for Greenland (green, accumulation zone only, Noël et al. (2018)) and Antarctica (orange) for all grid points with period-average seasonal surface melt of at least 5 mm w.e. Summer is defined as Nov–Feb in Antarctica and May–Aug in Greenland.

395 fore apply the temperature–SMAF relationship to the Greenland temperature distribu-
 396 tion.

397 Figure 5b shows the temperature deviation from T_c for Greenland. Similar to Fig. 5a,
 398 white areas indicate the regions where SMAF is currently most optimal for enhancing
 399 surface melt, red areas are too warm for a strong SMAF, and blue areas are currently
 400 too cold. In the current climate and based on our results from the AIS, it shows that SMAF
 401 is active in a large part of the interior ice sheet in southern Greenland, and a narrow band
 402 in the middle-elevated accumulation zone around the rest of the ice sheet. In a warm-
 403 ing climate, the SMAF region will migrate inland, corresponding to a right-ward shift
 404 of the green temperature distribution in Fig. 4. This leads to a rapid increase of the area
 405 being affected by SMAF when air temperatures over Greenland continue to rise.

406 5 Conclusions

407 In this study we investigate the spatial and temporal variability of the snowmelt–
 408 albedo feedback (SMAF) on the Antarctic ice sheet (AIS). This is done by performing
 409 two simulations with the regional atmospheric climate model RACMO2, covering the pe-
 410 riod 1979–2018. This model uses a parameterization that relates the surface albedo to
 411 the grain size of snow; by disabling the contribution of refrozen snow to albedo lower-
 412 ing, this allows us to explicitly model the effect of SMAF on surface melt. One simula-
 413 tion is performed with the full albedo parameterization (R_0), in the other simulation this
 414 refrozen-snow contribution is disabled (R_1). Following Jakobs et al. (2019), we define
 415 SMAF as the ratio of cumulative surface melt between these two simulations, a value
 416 of 1 indicating no effect, a value of X indicating that melt is enhanced X-fold because
 417 of SMAF.

418 We find that SMAF is spatially highly variable on the AIS, ranging from values close
 419 to 1 in cold, low-melt regions such as the Ross and Filchner-Ronne ice shelves, to val-
 420 ues up to 3 in coastal Dronning Maud Land (Fig. 2). Relating SMAF_t to average sum-
 421 mer (Nov–Feb) air temperature reveals a maximum around 265 K (T_c , Fig. 4). Many Antarc-
 422 tic ice shelves are located in the temperature regime where SMAF is currently optimal,
 423 except for the three largest ice shelves (Ross, Filchner-Ronne and Amery), which are too
 424 cold, and the entire Antarctic Peninsula (Fig. 5a), which is too warm.

Investigating the link between SMAF and the surface energy balance reveals that the timing of significant snowfall events with respect to surface melt is important. Seasonal SMAF is highest when melt occurs immediately after the last snowfall event at the onset of the melt season and in the absence of significant precipitation throughout the remainder of the season. The reason is that in this case the surface albedo is not reset to the new-snow value and enhanced melt occurs continuously. When snowfall is not immediately followed by surface melt, the surface albedo is lowered by dry snow metamorphism. The effect of refrozen snow on seasonal albedo is subsequently much smaller than in the previous example, and therefore SMAF is less important. In cold regions such as the Ross ice shelf, the air temperature is generally too low to accommodate continuous surface melt. When surface melt occurs, it is mostly constrained to a single melt day; as a result, SMAF is not able to significantly enhance surface melt. On Larsen C ice shelf, located in the mild AP, the air temperature is normally high enough to facilitate near-continuous surface melt; SMAF does enhance surface melt but it does not determine whether surface melt continues or ceases. This is contrary to moderate-temperature locations, where SMAF can be the determining factor for the start and continuation of surface melt.

Although a large part of Antarctica is currently too cold for an optimal SMAF, which occurs at ~ 265 K, rising temperatures in the future could expose even the largest ice shelves to a strong increase in surface melt because of SMAF. Applying the same threshold to the Greenland ice sheet shows that a large part of southern Greenland is in the SMAF-sensitive temperature regime (Fig. 5b), indicating that SMAF is an important driver for surface melt in that area.

Acknowledgments

This research has been supported by the Nederlandse Organisatie voor Wetenschappelijk Onderzoek (grant no. 866.15.204). Michiel van den Broeke acknowledges support from the Netherlands Earth System Science Centre (NESSC). We thank Brice Noël for carrying out the RACMO2.3p2 Greenland simulation. The data are available on <https://doi.org/10.5281/zenodo.3836044>. The authors declare no conflicts of interest.

References

- Agosta, C., Amory, C., Kittel, C., Orsi, A., Favier, V., Gallée, H., . . . Fettweis, X. (2019). Estimation of the antarctic surface mass balance using the regional climate model mar (1979-2015) and identification of dominant processes. *The Cryosphere*, *13*, 281-296. doi: 10.5194/tc-13-281-2019
- Alexander, P. M., LeGrande, A. N., Fischer, E., Tedesco, M., Fettweis, X., Kelley, M., . . . Schmidt, G. A. (2019). Simulated greenland surface mass balance in the giss mode2 gcm: Role of the ice sheet surface. *Journal of Geophysical Research: Earth Surface*, *124*, 750-765. doi: 10.1029/2018JF004772
- Bindschadler, R., Choi, H., Wichlacz, A., Bingham, R., Bohlander, J., Brunt, K., . . . Young, N. (2011). Getting around antarctica: new high-resolution mappings of the grounded and freely-floating boundaries of the antarctic ice sheet created for the international polar year. *The Cryosphere*, *5*, 569-588. doi: 10.5194/tc-5-569-2011
- Bisiaux, M. M., Edwards, R., McConnell, J. R., Curran, M. A. J., Van Ommen, T. D., Smith, A. M., . . . Taylor, K. (2012). Changes in black carbon deposition to antarctica from two high-resolution ice core records, 1850-2000 ad. *Atmospheric Chemistry and Physics*, *12*, 4107-4115. doi: 10.5194/acp-12-4107-2012
- Braun, M., Humbert, A., & Moll, A. (2009). Changes of wilkins ice shelf over the past 15 years and inferences on its stability. *The Cryosphere*, *3*, 41-56. doi: 10.5194/tc-3-41-2009
- Bromwich, D. H., Otieno, F. O., Hines, K. M., Manning, K. W., & Shilo, E. (2013).

- 476 Comprehensive evaluation of polar weather research and forecasting model
 477 performance in the antarctic. *Journal of Geophysical Research: Atmospheres*,
 478 *118*, 274-292. doi: 10.1029/2012JD018139
- 479 Cullather, R. I., Nowicki, S. M. J., Zhao, B., & Suarez, M. J. (2014). Evaluation
 480 of the surface representation of the greenland ice sheet in a general circulation
 481 model. *Journal of Climate*, *27*, 4835-4856. doi: 10.1175/JCLI-D-13-00635.1
- 482 ECMWF. (2008). IFS DOCUMENTATION - Cy33r1 - PART IV: PHYSI-
 483 CAL PROCESSES [Computer software manual]. Retrieved from [https://](https://www.ecmwf.int/en/eLibrary/9227-part-iv-physical-processes)
 484 www.ecmwf.int/en/eLibrary/9227-part-iv-physical-processes ([Online;
 485 accessed 6 June 2019])
- 486 Ettema, J., Van den Broeke, M. R., Van Meijgaard, E., Van de Berg, W. J., Box,
 487 J. E., & Steffen, K. (2010). Climate of the greenland ice sheet using a high-
 488 resolution climate model - part 1: Evaluation. *The Cryosphere*, *4*, 511-527.
 489 doi: 10.5194/tc-4-511-2010
- 490 Gardner, A. S., & Sharp, M. J. (2010). A review of snow and ice albedo and
 491 the development of a new physically based broadband albedo parameteriza-
 492 tion. *Journal of Geophysical Research: Earth Surface*, *115*(F01009). doi:
 493 10.1029/2009JF001444
- 494 Glasser, N. F., & Scambos, T. A. (2008). A structural glaciological analysis of the
 495 2002 larsen b ice-shelf collapse. *Journal of Glaciology*, *54*(184), 3-16. doi: 10
 496 .3189/002214308784409017
- 497 Grenfell, T. C., Warren, S. G., & Mullen, P. C. (1994). Reflection of solar radi-
 498 ation by the antarctic snow surface at ultraviolet, visible, and near-infrared
 499 wavelengths. *Journal of Geophysical Research*, *99*(D9), 18669-18684. doi:
 500 10.1029/94JD01484
- 501 Jakobs, C. L., Reijmer, C. H., Kuipers Munneke, P., König-Langlo, G., & Van den
 502 Broeke, M. R. (2019). Quantifying the snowmelt-albedo feedback at
 503 neumayer station, east antarctica. *The Cryosphere*, *13*, 1473-1485. doi:
 504 10.5194/tc-13-1473-2019
- 505 Jakobs, C. L., Reijmer, C. H., Smeets, C. J. P. P., Trusel, L. D., Van de Berg, W. J.,
 506 Van den Broeke, M. R., & Van Wessem, J. M. (2020). A benchmark dataset of
 507 in situ antarctic surface melt rates and energy balance. *Journal of Glaciology*,
 508 *66*(256), 291-302. doi: 10.1017/jog.2020.6
- 509 Jonsell, U. Y., Navarro, F. J., Bañón, M., Lapazaran, J. J., & Otero, J. (2012).
 510 Sensitivity of a distributed temperature-radiation index melt model based
 511 on aws observations and surface energy balance fluxes, hurd peninsula
 512 glaciers, livingston island, antarctica. *The Cryosphere*, *6*, 539-552. doi:
 513 10.5194/tc-6-539-2012
- 514 King, J. C., Gadian, A., Kirchgaessner, A., Kuipers Munneke, P., Lachlan-Cope,
 515 T. A., Orr, A., ... Weeks, M. (2015). Validation of the summertime surface
 516 energy budget of larsen c ice shelf (antarctica) as represented in three high-
 517 resolution atmospheric models. *Journal of Geophysical Research: Atmospheres*,
 518 *120*, 1335-1347. doi: 10.1002/2014JD022604
- 519 Kingslake, J., Ely, J. C., Das, I., & Bell, R. E. (2017). Widespread movement of
 520 meltwater onto and across antarctic ice shelves. *Nature*, *544*, 349-352. doi: 10
 521 .1038/nature22049
- 522 Kuipers Munneke, P., Van den Broeke, M. R., Lenaerts, J. T. M., Flanner, M. G.,
 523 Gardner, A. S., & Van de Berg, W. J. (2011). A new albedo parameterization
 524 for use in climate models over the antarctic ice sheet. *Journal of Geophysical*
 525 *Research: Atmospheres*, *116*(D05114). doi: 10.1029/2010JD015113
- 526 Lenaerts, J. T. M., Lhermitte, S., Drews, R., Ligtenberg, S. R. M., Berger, S., Helm,
 527 V., ... Pattyn, F. (2017). Meltwater produced by wind-albedo interaction
 528 stored in an east antarctic ice shelf. *Nature Climate Change*, *7*, 58-62. doi:
 529 10.1038/nclimate3180
- 530 Lenaerts, J. T. M., Van den Broeke, M. R., Déry, S. J., Van Meijgaard, E., Van de

- 531 Berg, W. J., Palm, S. P., & Sanz Rodrigo, J. (2012). Modeling drifting snow
 532 in antarctica with a regional climate model: 1. methods and model evalu-
 533 ation. *Journal of Geophysical Research: Atmospheres*, *117*(D05108). doi:
 534 10.1029/2011JD016145
- 535 Marquetto, L., Kaspari, S., & Simões, J. C. (2020). Refractory black carbon (rbc)
 536 variability in a 47-year west antarctic snow and firn core. *The Cryosphere*, *14*,
 537 1537-1554. doi: tc-14-1537-2020
- 538 Massom, R. A., Scambos, T. A., Bennetts, L. G., Reid, P. A., Squire, V. A., &
 539 Stammerjohn, S. E. (2018). Antarctic ice shelf disintegration triggered
 540 by sea ice loss and ocean swell. *Nature*, *558*, 383-389. doi: 10.1038/
 541 s41586-018-0212-1
- 542 Morlighem, M., Rignot, E., Binder, T., Blankenship, D. D., Drews, R., Eagles, G.,
 543 ... Young, D. A. (2020). Deep glacial troughs and stabilizing ridges un-
 544 veiled beneath the margins of the antarctic ice sheet. *Nature Geoscience*, *13*,
 545 132-137. doi: 10.1038/s41561-019-0510-8
- 546 Noël, B. P. Y., Van de Berg, W. J., Van Wessem, J. M., Van Meijgaard, E., Van As,
 547 D., Lenaerts, J. T. M., ... Van den Broeke, M. R. (2018). Modelling the cli-
 548 mate and surface mass balance of polar ice sheets using racmo2, part 1: Green-
 549 land (1958-2016). *The Cryosphere*, *12*, 811-831. doi: 10.5194/tc-12-811-2018
- 550 Padman, L., Costa, D. P., Dinniman, M. S., Fricker, H. A., Goebel, M. E., Huck-
 551 stadt, L. A., ... Van den Broeke, M. R. (2012). Oceanic controls on the
 552 mass balance of wilkins ice shelf, antarctica. *Journal of Geophysical Research*,
 553 *117*(C01010). doi: 10.1029/2011JC007301
- 554 Pritchard, H. D., Ligtenberg, S. R. M., Fricker, H. A., Vaughan, D. G., Van den
 555 Broeke, M. R., & Padman, L. (2012). Antarctic ice-sheet loss driven by basal
 556 melting of ice shelves. *Nature*, *484*, 502-505. doi: 10.1038/nature10968
- 557 Reijmer, C. H., Van Meijgaard, E., & Van den Broeke, M. R. (2005). Evaluation of
 558 temperature and wind over antarctica in a regional atmospheric climate model
 559 using 1 year of automatic weather station data and upper air observations.
 560 *Journal of Geophysical Research*, *110*(D04103). doi: 10.1029/2004JD005234
- 561 Rott, H., Müller, F., Nagler, T., & Floricioiu, D. (2011). The imbalance of glaciers
 562 after disintegration of larsen-b ice shelf, antarctic peninsula. *The Cryosphere*,
 563 *5*, 125-134. doi: 10.5194/tc-5-125-2011
- 564 Scambos, T. A., Bohlander, J. A., Shuman, C. A., & Skvarca, P. (2004).
 565 Glacier acceleration and thinning after ice shelf collapse in the larsen b
 566 embayment, antarctica. *Geophysical Research Letters*, *31*(L18402). doi:
 567 10.1029/2004GL020670
- 568 Shepherd, A., Ivins, E. R., Rignot, E., Smith, B., Van den Broeke, M. R., Velicogna,
 569 I., ... Wouters, B. (2018). Mass balance of the antarctic ice sheet from 1992
 570 to 2017. *Nature*, *558*, 219-222. doi: 10.1038/s41586-018-0179-y
- 571 Souverijns, N., Gossart, A., Demuzere, M., Lenaerts, J. T. M., Medley, B., Gorodet-
 572 skaya, I. V., ... Van Lipzig, N. P. M. (2019). A new regional climate model for
 573 polar-cordex: Evaluation of a 30-year hindcast with cosmo-clm² over antarcti-
 574 ca. *Journal of Geophysical Research: Atmospheres*, *124*, 1405-1427. doi:
 575 10.1029/2018JD028862
- 576 Trusel, L. D., Frey, K. E., Das, S. B., Karnauskas, K. B., Kuipers Munneke, P.,
 577 Van Meijgaard, E., & Van den Broeke, M. R. (2015). Divergent trajectories of
 578 antarctic surface melt under two twenty-first-century climate scenarios. *Nature*
 579 *Geoscience*, *8*, 927-934. doi: 10.1038/NCEO2563
- 580 Turner, J., Orr, A., Gudmundsson, G. H., Jenkins, A., Bingham, R. G., Hillenbrand,
 581 C.-D., & Bracegirdle, T. J. (2017). Atmosphere-ocean-ice interactions in
 582 the amundsen sea embayment, west antarctica. *Reviews of Geophysics*, *55*,
 583 235-276. doi: 10.1002/2016RG000532
- 584 Undén, P., Rontu, L., Järvinen, H., Lynch, P., Calvo, J., Cats, G., ... Tijm, A.
 585 (2002). Hirlam-5 scientific documentation [Computer software manual].

- Retrieved from <http://hirlam.org/index.php/hirlam-documentation/doc/download/308-unden-et-al-2002> ([Online; accessed 25 January 2017])
- 586
587
588 Van Dalum, C. T., Van de Berg, W. J., Libois, Q., Picard, G., & Van den Broeke,
589 M. R. (2019). A module to convert spectral to narrowband snow albedo for
590 use in climate models: Snowbal v1.2. *Geoscientific Model Development*, *12*,
591 5157-5175. doi: 10.5194/gmd-12-5157-2019
- 592 Van de Berg, W. J., & Medley, B. (2016). Brief communication: Upper-air re-
593 laxation in racmo2 significantly improved modelled interannual surface
594 mass balance variability in antarctica. *The Cryosphere*, *10*, 459-463. doi:
595 10.5194/tc-10-459-2016
- 596 Van den Broeke, M. R. (2005). Strong surface melting preceded collapse of antarctic
597 peninsula ice shelf. *Geophysical Research Letters*, *32*(L12815). doi: 10.1029/
598 2005GL023247
- 599 Van den Broeke, M. R., Reijmer, C. H., Van As, D., Van de Wal, R. S. W., &
600 Oerlemans, J. (2005). Seasonal cycles of antarctic surface energy balance
601 from automatic weather stations. *Annals of Glaciology*, *41*, 131-139. doi:
602 10.3189/172756405781813168
- 603 Van den Broeke, M. R., Van As, D., Reijmer, C. H., & Van de Wal, R. S. W. (2005).
604 Sensible heat exchange at the antarctic snow surface: a study with automatic
605 weather stations. *International Journal of Climatology*, *25*, 1081-1101. doi:
606 10.1002/joc.1152
- 607 Van Kampenhout, L., Lenaerts, J. T. M., Lipscomb, W. H., Sacks, W. J., Lawrence,
608 D. M., Slater, A. G., & Van den Broeke, M. R. (2017). Improving the rep-
609 resentation of polar snow and firn in the community earth system model.
610 *Journal of Advances in Modeling Earth Systems*, *9*, 2583-2600. doi:
611 10.1002/2017MS000988
- 612 Van Wessem, J. M., Van de Berg, W. J., Noël, B. P. Y., Van Meijgaard, E., Birn-
613 baum, G., Jakobs, C. L., ... Van den Broeke, M. R. (2018). Modelling
614 the climate and surface mass balance of polar ice sheets using RACMO2,
615 part 2: Antarctica (1979-2016). *The Cryosphere*, *12*, 1479-1498. doi:
616 10.5194/tc-2017-202
- 617 Warren, S. G., & Clarke, A. D. (1990). Soot in the atmosphere and snow surface of
618 antarctica. *Journal of Geophysical Research*, *95*(D2), 1811-1816. doi: 10.1029/
619 JD095iD02p01811
- 620 Wiesenekker, J. M., Kuipers Munneke, P., Van den Broeke, M. R., & Smeets,
621 C. J. P. P. (2018). A multidecadal analysis of föhn winds over larsen c ice
622 shelf from a combination of observations and modeling. *Atmosphere*, *9*, 172.
623 doi: 10.3390/atmos9050172
- 624 Wiscombe, W. J., & Warren, S. G. (1980). A model for the spectral albedo of snow.
625 i: Pure snow. *Journal of the Atmospheric Sciences*, *37*, 2712-2733. doi: 10
626 .1175/1520-0469(1980)037<2712:AMFTSA>2.0.CO;2
- 627 Wouters, B., Martín-Español, A., Helm, V., Flament, T., Van Wessem, J. M.,
628 Ligtenberg, S. R. M., ... Bamber, J. L. (2015). Dynamic thinning of
629 glaciers on the southern antarctic peninsula. *Science*, *348*(6237), 899-903.
630 doi: 10.1126/science.aaa5727